Journal of Molecular Liquids 389 (2023) 122832

Contents lists available at ScienceDirect

Journal of Molecular Liquids

journal homepage: www.elsevier.com/locate/molliq

Enhanced degradation of Ionic liquid 1-n-Butyl-3-Methylimidazolium chloride by visible Light-Promoted Fe-MOF-activated Peroxydisulfate: A comparative study with DFT and Eco-Toxicity assessment

Tran Doan Trang [a], Eilhann Kwon [b], Jet-Chau Wen [c,d], Nguyen Nhat Huy [e,f], Venkata Subbaiah Munagapati [c], Suresh Ghotekar [g], Kuo-Pin Yu [h,*], Kun-Yi Andrew Lin [a,i,*]

[a] Department of Environmental Engineering & Innovation and Development Center of Sustainable Agriculture & Research Center of Sustainable Energy and Nanotechnology, National Chung Hsing University, 250 Kuo-Kuang Road, Taichung, Taiwan
[b] Department of Earth Resources and Environmental Engineering, Hanyang University, SeongDong-Gu, Seoul, Republic of Korea
[c] Research Centre for Soil & Water Resources and Natural Disaster Prevention (SWAN), National Yunlin University of Science and Technology, Douliou, Yunlin 64002, Taiwan, ROC
[d] Department of Safety, Health, and Environmental Engineering, National Yunlin University of Science and Technology, Douliou, Yunlin 64002, Taiwan, ROC
[e] Faculty of Environment and Natural Resources, Ho Chi Minh City University of Technology (HCMUT), Ho Chi Minh City 700000, Viet Nam
[f] Vietnam National University Ho Chi Minh City, Ho Chi Minh City 700000, Viet Nam
[g] Centre for Herbal Pharmacology and Environmental Sustainability, Chettinad Hospital and Research Institute, Chettinad Academy of Research and Education, Kelambakkam 603103, Tamil Nadu, India
[h] Institute of Environmental and Occupational Health Sciences, National Yang Ming Chiao Tung University, Taipei 11221, Taiwan
[i] Institute of Analytical and Environmental Sciences, National Tsing Hua University, Hsinchu, Taiwan

ARTICLE INFO

Keywords:
Ionic liquid
Persulfate
MOFs
Photocatalysis
Sulfate radicals
ECOSAR

ABSTRACT

Ionic liquids (ILs) are increasingly adopted in various applications, leading to their release into the water environment, where they pose potential threats to ecology in view of toxicities. In order to remove 1-n-Butyl-3-Methylimidazolium (BMI) chloride, a well-known model IL, from water, urgent and crucial techniques are needed. Peroxydisulfate (PDS) activated by heterogeneous catalysts is useful for BMI degradation; nonetheless, heterogeneously activated PDS has been utilized in very few studies. A Fe-based metal–organic framework, Fe-2-aminobenzene-1,4-dicarboxylic acid (FeBDC-NH_2), is suggested here for serving as an activator because of its Fe sites, high surface areas, porosities, and visible-light responsive photocatalytic activity. The structure–property relationship of FeBDC-NH_2 in PDS activation is compared to that of Fe-Benzene-1,4-dicarboxylic acid (FeBDC), and both are found to activate PDS to degrade BMI. FeBDC-NH_2, however, significantly accelerated BMI degradation when exposed to visible light. Compared to activation energies reported by other oxidation approaches, the activation energy of BMI degradation is considerably lower. Through theoretical DFT calculations, the mechanism and pathway of BMI degradation by FeBDC-NH_2/PDS are examined. The eco-toxicities of BMI degradation intermediates are researched to understand the impact of BMI degradation on the environment. These analyses show that the toxicities of BMI are effectively reduced by FeBDC-NH_2-activated PDS under light irradiation and that the final derivatives of BMI produced during the degradation process are non-harmful in terms of both acute and chronic toxicities.

1. Introduction

A novel class of molten salts categorized as “Ionic Liquids” (ILs) can exhibit fluid characteristics under normal circumstances and also show nearly minimal vapor pressure at room temperature. Consequently, ILs are increasingly used as green chemicals as well as functional components for various applications [1,2]. Nevertheless, due to rising usage in a variety of processes, ILs have been discharged into aquatic environments [3], endangering ecology due to their toxicity [4]. Therefore, developing practical methods for eliminating the ILs from contaminated water is essential.

Conventionally, imidazolium and pyridinium are the two main

* Corresponding authors.
E-mail addresses: kpyu03@nycu.edu.tw (K.-P. Yu), linky@nchu.edu.tw (K.-Y.A. Lin).

https://doi.org/10.1016/j.molliq.2023.122832
Received 23 April 2023; Received in revised form 1 August 2023; Accepted 12 August 2023
Available online 15 August 2023

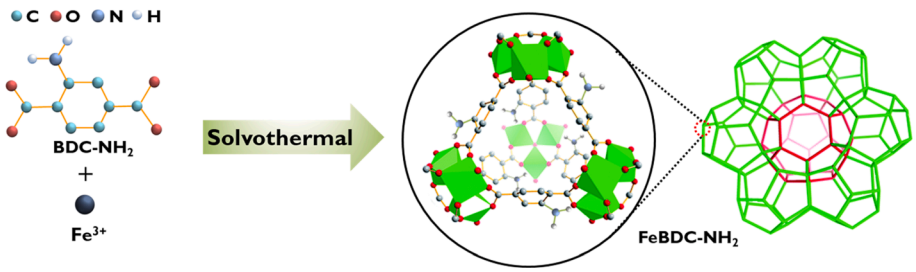

Fig. 1. Preparation scheme for FeBDC-NH_2.

classes of cations in ILs; imidazolium-bearing ILs, consisting of imidazolate and R_4N^+ groups, are even the most prevalent category among all of these ILs [5,6]. In particular, 1-n-Butyl-3-Methylimidazolium (BMI) is a widely-employed cation in ILs, making BMI a model IL [7–9]. Therefore, it is crucial to develop effective techniques for removing BMI from contaminated aquatic environments.

Even though several physiochemical methods [7,10] have been investigated for the removal of BMI, oxidation appears to be the most advantageous method since it would decompose BMI to lessen its adverse effects [11]. For the degradation of BMI in water, a number of oxidation methods, including various types of Fenton's processes [11–13], have been proposed. These procedures often require the addition of hydrogen peroxide along with homogenous, non-recyclable catalysts (such as Fe^{2+}), which makes them less practical. In order to degrade BMI, it would be desirable to design heterogeneous catalytic methods.

Due to the high oxidation potentials and reaction selectivities of the sulfate radical ($SO_4^{\bullet-}$), $SO_4^{\bullet-}$-based oxidation techniques have gained increasing attention in recent years [14]. These $SO_4^{\bullet-}$-based oxidation techniques can be used to detoxify BMI-contaminated water. Peroxydisulfate (PDS), which is industrially available, affordable, and easily accessible, has been the most preferred and often used reagent for producing $SO_4^{\bullet-}$. Thus, employing PDS to eliminate BMI from water would undoubtedly be promising. However, research on BMI degradation by PDS-related mechanisms is quite limited. The most practical and effective method for activating PDS has been determined to be the use of

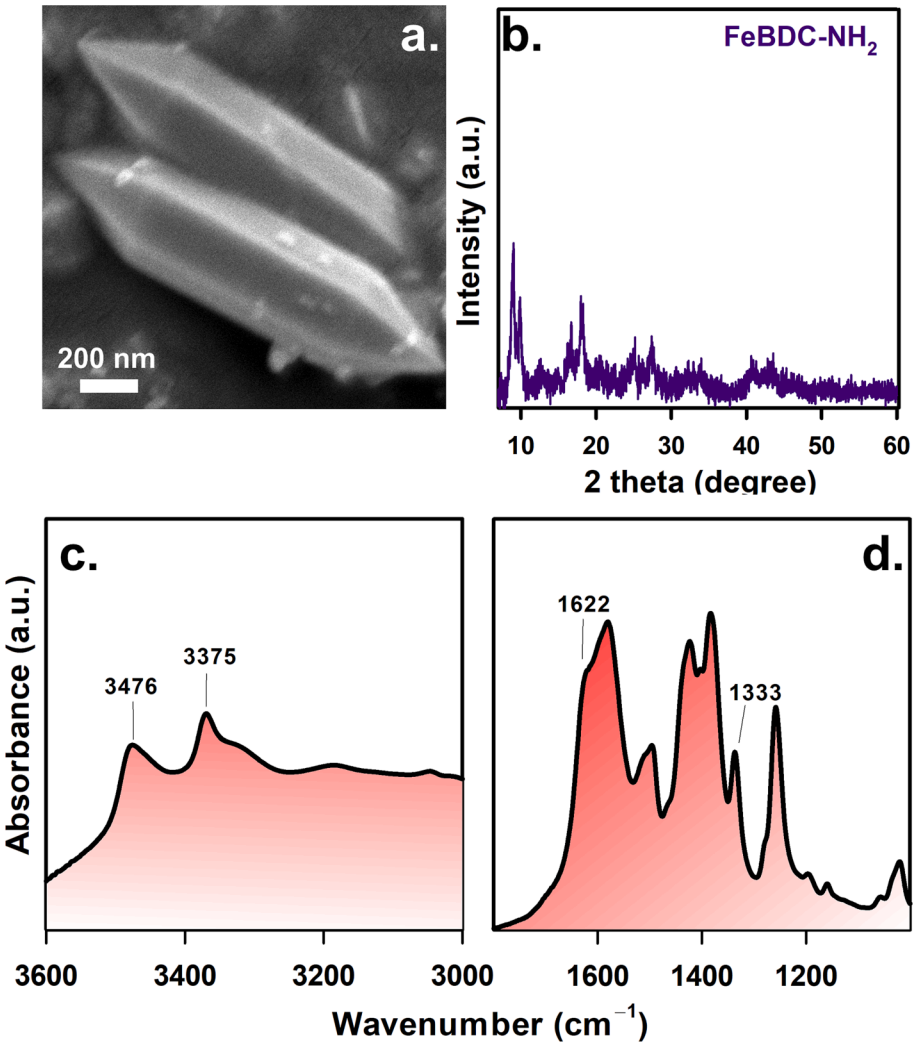

Fig. 2. (a). A SEM image, (b). XRD patterns, (c-d). FTIR spectrum of FeBDC-NH_2.

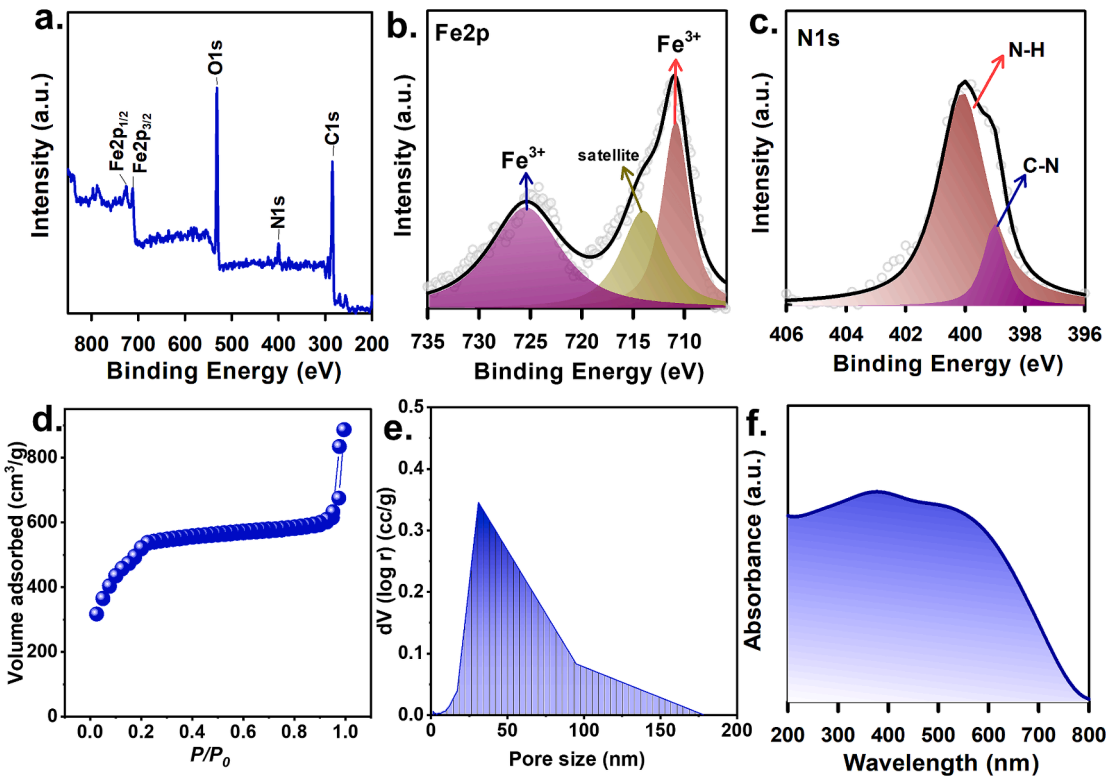

Fig. 3. (a-c). XPS spectra of FeBDC-NH_2; (d). N_2 sorption and (e) pore size distribution of FeBDC-NH_2, (f). DRS spectrum of FeBDC-NH_2.

heterogeneous catalysts [15–19]. For instance, Ding and his team created Fe_3O_4 nanoparticles (NPs) to activate PDS for eliminating toxicants from water [20]. Nevertheless, it has been demonstrated that NPs can substantially agglomerate, particularly in aquatic phases, reducing the reactive surfaces and activities [21].

In contrast to traditional iron NPs, this study would introduce using Metal-Organic Frameworks (MOFs), a novel family of nanoscale heterogeneous metal-coordinated materials, to activate PDS. MOFs can contain transition metals coordinating with organic ligands, and their superior textural properties and versatility, enabling intriguing heterogeneous catalysts for a wide range of applications. As a result, Fe-bearing MOFs are already investigated for their ability to catalyze oxidants for the degradation of toxic contaminants [22]. Nonetheless, no Fe-based MOFs have ever been employed for PDS activation to degrade BMI; therefore, the purpose of this research is to study Fe-based MOFs for PDS activation in order to eliminate BMI.

In this study, a Fe-based MOF composed of Fe and 2-aminobenzene-1,4-dicarboxylic acid (BDC-NH_2), forming FeBDC-NH_2, was chosen because FeBDC-NH_2 has a much higher surface area, porosity, and structural stability than other types of Fe-based MOFs [23]. Furthermore, FeBDC-NH_2 is functionalized with an amine group. By incorporating the –NH_2 group, FeBDC-NH_2 possesses photo-catalytic properties, especially under visible light [24], allowing FeBDC-NH_2 to be both a chemical catalyst and a photocatalyst. By these dual functions, FeBDC-NH_2 is expected to be a useful activator for PDS in BMI degradation. Because almost no research is reported to look into the catalytic properties of FeBDC-NH_2 in PDS activation to eliminate BMI, this report is the first research of Fe-based MOFs with NH_2 to activate PDS for eliminating BMI under visible light irradiation.

More importantly, a Fe-Benzene-1,4-dicarboxylic acid (FeBDC) analogue without the amine group would be synthesized and directly compared with FeBDC-NH_2 for comparisons to unravel the structure–property relationship of FeBDC-NH_2 in PDS activation during BMI degradation. Moreover, the corresponding decomposition process of BMI using FeBDC-NH_2 + PDS with irradiation is investigated by analytic studies and computational explorations. Besides, eco-toxicity evaluation of possible intermediates would also be performed to examine the variation of acute and chronic eco-toxicities along the process of BMI degradation to investigate the environmental implication of BMI degradation.

2. Experimental

The reagents utilized here were gained directly from reagent suppliers. Fig. 1 depicts the solvothermal process used to synthesize FeBDC-NH_2. The preparation technique, BMI degradation by PDS, analytic procedures, and computer-aided computing details are all included in the supplemental material (SM).

3. Results and discussion

3.1. Physical and chemical properties of FeBDC-NH_2

Firstly, the morphology of FeBDC-NH_2 was examined (Fig. 2(a)), and it showed a hexagonal geometry that was compatible with the described morphology of FeBDC-NH_2 in the literature [24], indicating that FeBDC-NH_2 was successfully synthesized. Next, the XRD pattern of FeBDC-NH_2 was also measured (Fig. 2(b)) and it was highly comparable to the reported one in the literature [25], suggesting that the as-synthesized FeBDC-NH_2 was well formulated and prepared. The infrared spectroscopic analysis of FeBDC-NH_2 is shown in Fig. 2(c), which closely agreed with the reported infrared spectrum of FeBDC-NH_2 with numerous noteworthy bands [24]. Specifically, two separate bands formed from BDC-NH_2 were detected at 1339 and 1625 cm^{-1}, which, respectively, correspond to ν (C-N) and σ (N–H) bonds. Besides, two other bands at 3378 and 3475 cm^{-1} could be used for identifying the stretching modes of the –NH_2 group [24].

Next, FeBDC-NH_2 would be then investigated using X-ray photoelectron spectroscopy (XPS) (Fig. 3). Fe, C, N, and O were distinguished in the survey of FeBDC-NH_2 (Fig. 3(a)). The XPS characterization

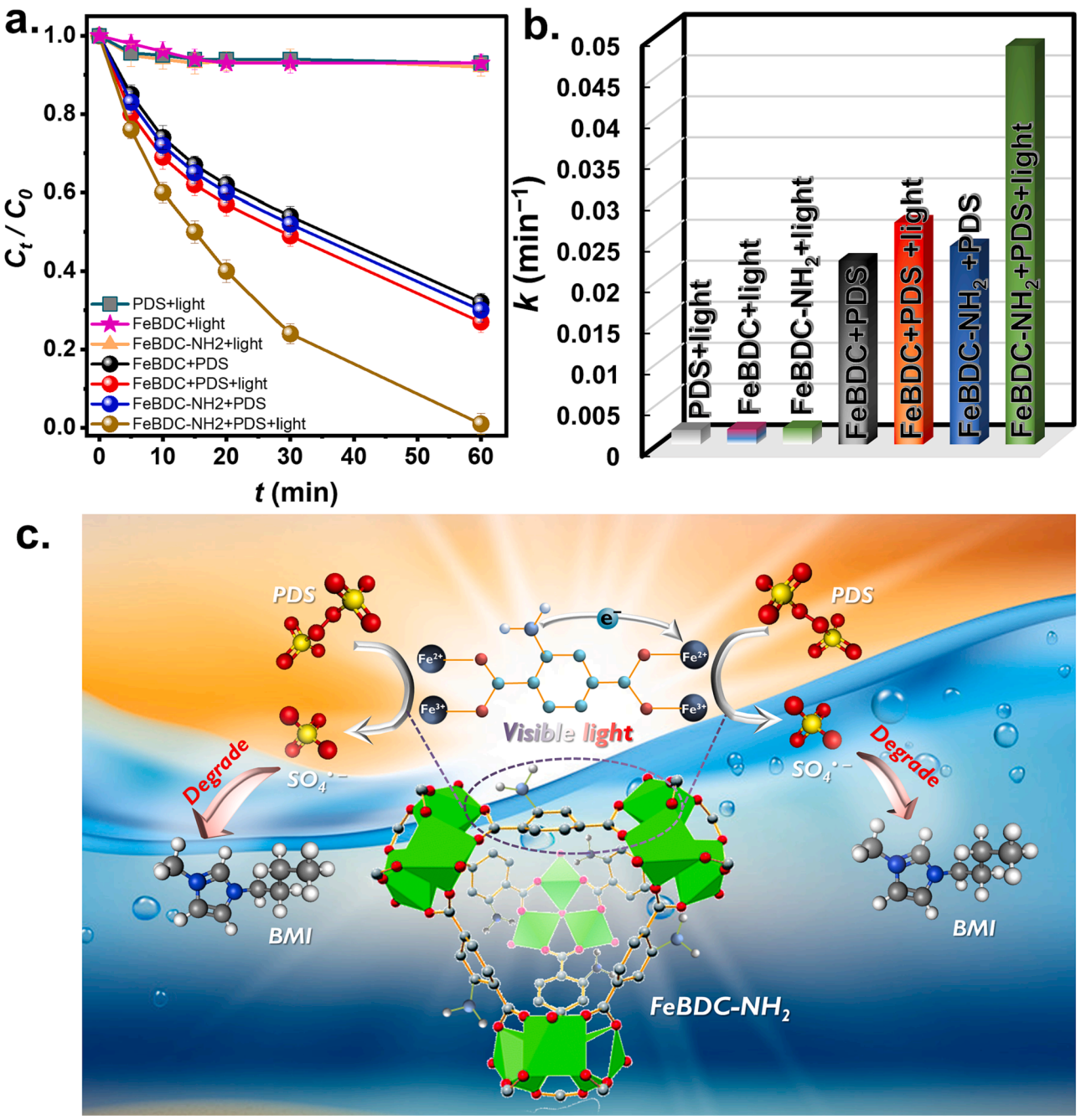

Fig. 4. (a) Comparison of degradation of BMI and (b) corresponding rate constants of BMI degradation (Catalyst = 100 mg/L, PDS = 100 mg/L,T = 30 °C); (c) a potential catalytic mechanism of FeBDC-NH_2 under visible light.

successfully verified that FeBDC-NH_2 contained both the amino group and Fe site. Then, in Fig. 3(b), the Fe2p spectrum would be analyzed to show a number of bands that originated from Fe^{3+}, corroborating that the Fe species had not changed in FeBDC-NH_2, as the theoretical Fe species of FeBDC-NH_2 or FeBDC would be Fe^{3+} [26].

Deconvolution was also performed on the N1s (Fig. 3(c)), which contained two different bands. The band at 399.3 eV, which would be attributable to the N-C in FeBDC-NH_2, and the band at 400.2 eV, which would be ascribed to the N–H group in FeBDC-NH_2, respectively, confirm the amine functional group of FeBDC-NH_2 [27–29].

In addition, the surface area of FeBDC-NH_2 was assessed, and the volumetric N_2 sorption is displayed in Fig. 3(d), which would be comparable to the IUPAC VI-typed isotherm, enabling it to exhibit a high surface area of 1200 m^2/g.

The FeBDC-NH_2 was then subjected to diffuse reflectance spectroscopy (DRS) analysis, which should demonstrate photocatalytic activities, particularly visible-light sensitive photocatalytic activities. For comparison, FeBDC was synthesized, and its image and XRD pattern (Fig. S1 in the supplementary materials) matched those of previously reported FeBDC; the DRS of FeBDC would be characterized (Fig. S2) to exhibit the absorption spectrum ranging from 260 to 610 nm. In contrast to the spectra of FeBDC, FeBDC-NH_2 absorbed a more extensive region of light than FeBDC (Fig. 3(f)) from 260 to 810 nm. Furthermore, the amine-functionalized organic ligand and the Fe_3O structure of the FeBDC-NH_2 then contributed to the light absorption in the 310 to 800 nm region [30].

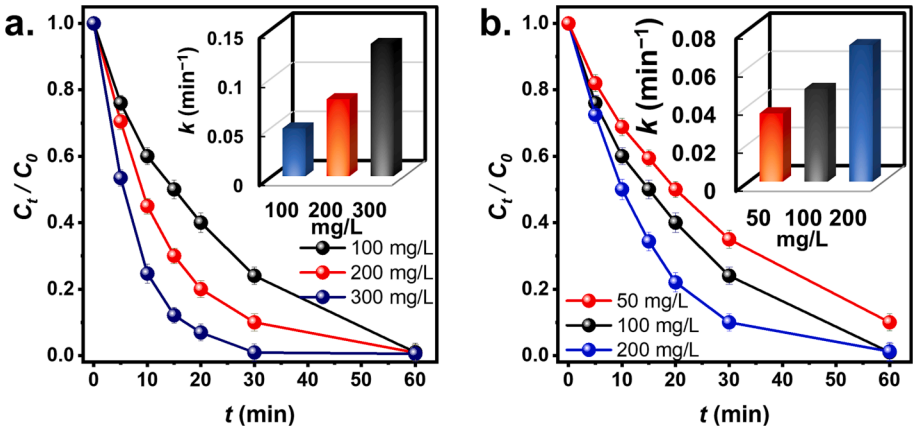

Fig. 5. Effects of (a) catalyst dosage and (b) PDS dosage on BMI degradation and rate constants (Catalyst = 100 mg/L, PDS = 100 mg/L,T = 30 °C).

3.2. Degradation of BMI by PDS

BMI degradation was then examined using PDS activated by catalysts (a) in Fig. 4. When FeBDC-NH_2 was exposed to visible light without the addition of PDS, the degradation of BMI appeared to be extremely minimal, while C_t/C_0 only reached 0.95 after 1 h. This implies that BMI adsorption to FeBDC-NH_2 was negligible, and the photocatalytic degradation of BMI by FeBDC-NH_2 was also insignificant. Next, when PDS alone was used under light irradiation, BMI was barely degraded, implying that PDS under visible light irradiation was ineffective and that additional useful activation strategies for PDS were required. When FeBDC-NH_2 was mixed with PDS without being exposed to light, the variation of BMI was visibly lowered, and its C_t/C_0 reached 0.3 after 1 h. Because FeBDC-NH_2 and PDS were impotent separately for degrading.

BMI even under light irradiation, this phenomenon suggests that FeBDC-NH_2 enabled the activation of PDS to potentially produce reactive oxygen species (ROS) for degrading BMI even without light irradiation because Fe^{3+} is capable of catalyzing decomposition of PDS for producing ROS via the following equations (Eqs. (1)-(3)) [31]:

$$Fe^{2+}@FeBDC\text{-}NH_2 + S_2O_8^{2-} \rightarrow Fe^{3+}@FeBDC\text{-}NH_2 + SO_4^{\bullet -} + SO_4^{2-} \quad (1)$$

Fe^{3+} can also further react with $S_2O_8^{2-}$ to transfer back to Fe2 + as follows:

$$Fe^{3+}@FeBDC\text{-}NH_2 + S_2O_8^{2-} \rightarrow Fe^{3+}@FeBDC\text{-}NH_2 + S_2O_8^{\bullet -} \quad (2)$$

The resulting $SO_4^{\bullet -}$ as well as other ROS can attack BMI and cause degradation of BMI.

Furthermore, after visible light irradiation was applied, the combination of FeBDC-NH_2, PDS, and light irradiation led to the rapid degradation of BMI, resulting in the complete removal of BMI in 60 min. This shows that the visible light irradiation increased PDS activation, which in turn enhanced BMI degradation. The variation of total organic carbon (TOC) of BMI degradation by FeBDC-NH_2-activated PDS with and without light irradiation was also investigated in Fig. S3. In both cases, TOC certainly decreased at the increasing reaction time, demonstrating that BMI was certainly decomposed by FeBDC-NH_2-activated PDS. In addition, the light irradiation would also enhance the TOC removal, validating that the light irradiation would enhance the decomposition of BMI.

To better understand the mechanism, FeBDC (without the NH_2 moiety) was also evaluated, and the combination of FeBDC and PDS also caused significant BMI degradation; however, light irradiation hardly improved the BMI degradation by FeBDC + PDS.

The pseudo 1st order equation would be then used to quantify degradation rates under various conditions by the following equation to quantitatively compare BMI degradation by these catalysts [32–36]:

$$C_t = C_0 e^{-kt} \quad (3)$$

where k is the "apparent" rate constant. Fig. 4(b) summarizes the rate constants of various catalysts. Because PDS + light, FeBDC + light, and FeBDC-NH_2 + light all had very low k values, the combinations of FeBDC and FeBDC-NH_2 with PDS all resulted in BMI degradation regardless of visible light irradiation.

While both FeBDC-NH_2 and FeBDC activated PDS to degrade BMI, visible light irradiation significantly increased BMI degradation by FeBDC-NH_2 rather than FeBDC. The k of BMI elimination by FeBDC + PDS was 0.022 min^{-1}, which was marginally improved to 0.027 min^{-1} under light irradiation. Nonetheless, the k of BMI degradation by FeBDC-NH_2 + PDS was 0.024 min^{-1}, which would significantly rise to 0.049 min^{-1} under visible light irradiation, indicating that FeBDC-NH_2 would be a more beneficial activator than FeBDC for PDS activation to eliminate BMI.

When FeBDC-NH_2 alone was irradiated by visible light, the pseudo first order rate constant was calculated as 0.002 min^{-1}, indicating that if no oxidant (i.e., PDS) was used, the photocatalysis of BMI by FeBDC-NH_2 itself was very marginal. On the other hand, when FeBDC-NH_2 was combined with PDS (without light), the BMI degradation proceeded much faster with a rate constant of 0.024 min^{-1}. This suggests that the activated PDS would contribute considerably to BMI degradation, whereas FeBDC-NH_2-activated PDS under light would lead to a rate constant of 0.049 min^{-1}, demonstrating that photocatalysis by FeBDC-NH_2 for additional activation of PDS seemed to also play an important role. Because FeBDC-NH_2 contains the NH_2 group, this NH_2 moiety would absorb irradiation for transferring an electron from BDC-NH_2 to the iron-oxide group, converting Fe^{3+} of FeBDC-NH_2 to Fe^{2+} for activating PDS to create $SO_4^{\bullet -}$ [37] and accelerating BMI degradation. Thus, the significantly accelerated BMI degradation by FeBDC-NH_2-activated PDS under light irradiation could be attributable to the two processes indicated above in Fig. 4(c).

3.3. Influences of catalyst and PDS on BMI elimination

Although FeBDC-NH_2 combined with PDS efficiently eliminated BMI, it would be vital to study their distinct contributions to BMI degradation. As a result, the effects of FeBDC-NH_2 and PDS concentrations on BMI elimination would be examined. Fig. 5(a) shows BMI elimination by FeBDC-NH_2 at various doses from 100 to 300 mg/L, and FeBDC-NH_2 at three dosages degraded BMI rather efficiently in 60 min. This finding indicates that FeBDC-NH_2 with visible light has a very strong catalytic activity to expedite PDS activation even at a low FeBDC-NH_2 dosage of 100 mg/L, which would still activate PDS for complete BMI degradation.

However, the elimination rates were clearly distinct with the various

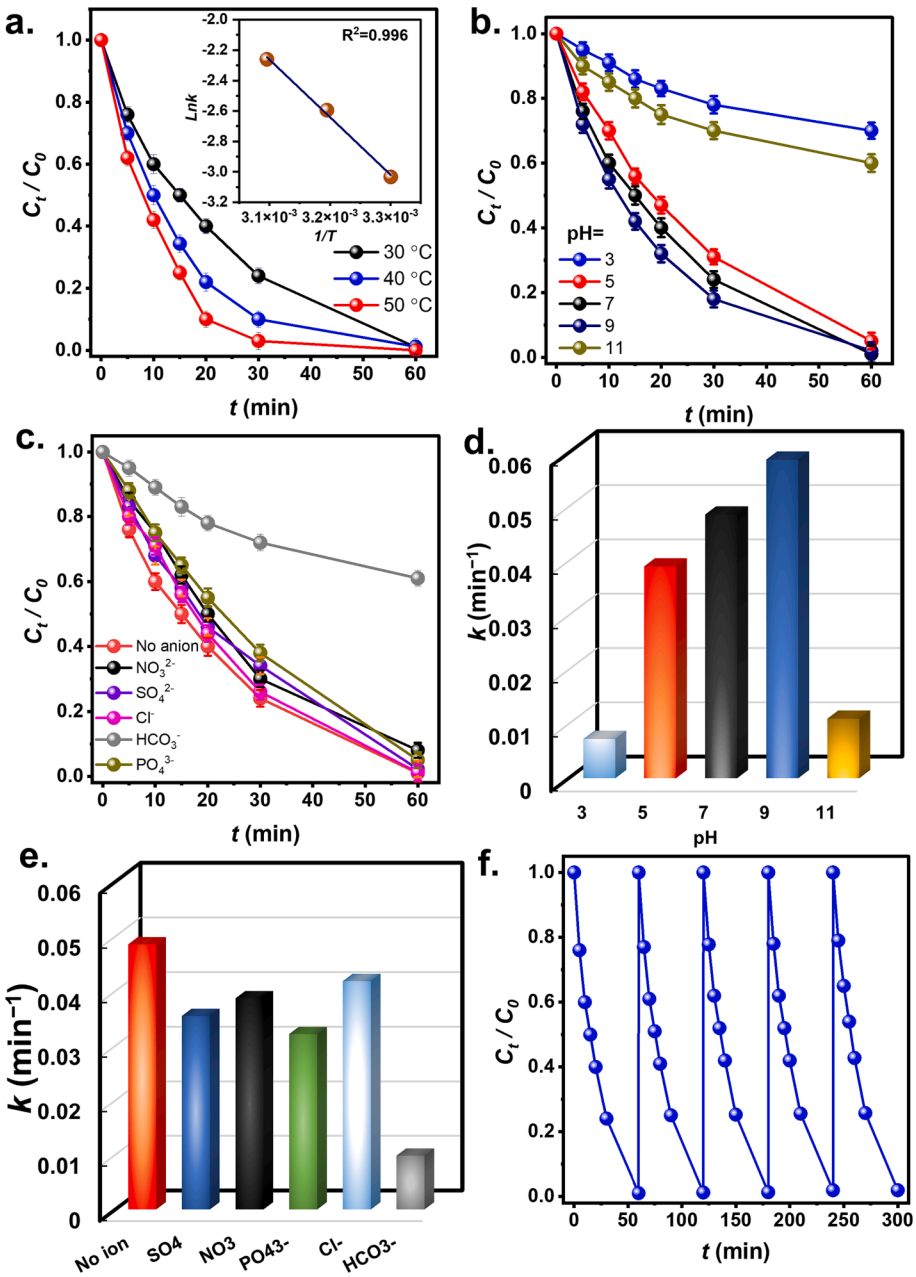

Fig. 6. Effects of various factors on BMI degradation by FeBDC-NH_2 + PDS under visible light: (a) temperature, (b) pH, (c) ions and (d),(e) corresponding rate constants; (f) recyclability test.

catalyst dosages. When FeBDC-NH_2 was from 100 to 200 mg/L, the k changed from 0.049 to 0.078 min^{-1} and then to 0.134 min^{-1} when FeBDC-NH_2 was elevated to 300 mg/L. The result implies that a higher FeBDC-NH_2 dose speeded up BMI elimination via increasing $SO_4^{\bullet-}$ or other ROS production from PDS with more reactive catalysts.

In addition, BMI elimination by PDS with different concentrations would be examined in Fig. 5. (b). When PDS concentration increased from 50 to 100 mg/L, BMI degradation improved significantly when k rose from 0.036 to 0.049 min^{-1}. As the PDS dose increased to 200 mg/L, the degradation rate increased to 0.072 min^{-1}. These findings also show that a higher PDS concentration accelerates BMI deterioration. Nonetheless, in the case of PDS = 50 mg/L, BMI was not completely eradicated since C_t/C_0 after 60 min was only 0.12. This indicates that the lower PDS dosage resulted in insufficient BMI degradation, probably due to insufficient $SO_4^{\bullet-}$ or ROS produced from the lower amount of PDS. These analyses also show that the level of BMI degradation was more responsive to PDS doses because $SO_4^{\bullet-}$ was formed from PDS rather than FeBDC-NH_2. FeBDC-NH_2, on the other hand, worked as an activator to modulate the rates [38,39].

3.4. Influences of temperature and pH on BMI elimination

BMI degradation by FeBDC-NH_2-activated PDS at 30, 40, and 50 °C is shown in Fig. 6(a). BMI was completely removed by FeBDC-NH_2-activated PDS under visible light irradiation at all studied temperatures; however, the elimination was more rapid at elevated temperatures. As the reaction was from 30 to 40 and 50 °C, k rose significantly from 0.049 to 0.075 and 0.104 min^{-1}, indicating that elevated temperatures improved BMI elimination.

The k was further associated with temperatures by using the following equation (Eq.(4)):

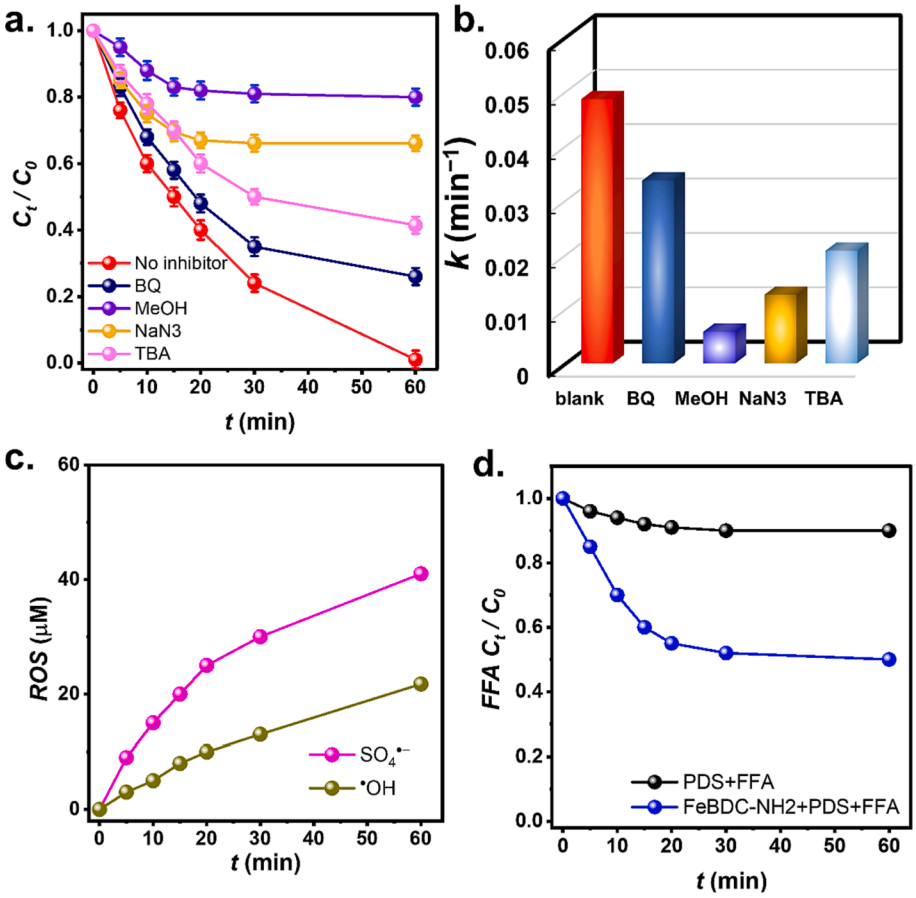

Fig. 7. Effects of various factors on BMI degradation:(a) probe agents and (b)corresponding rate constants; (c) concentrations of $SO_4^{\bullet-}$ and •OH, and (d) consumption of FFA.

$$Lnk = lnA - E_a/RT \quad (4)$$

where *Ea* represents the activation energy (*Ea*, kJ mol^{-1}) of BMI degradation.

A plot of *1/T* vs. Ln $_k$ based on Eq. (4) is also given and the *Ea* was calculated to be 31.5 kJ/mol. A previous study also observed the degradation of BMI by Fe^{3+} employing a H2O2-based oxidation process, resulting in a substantially larger *Ea* = 43.3 kJ/mol [40], validating that FeBDC-NH2-activated PDS would be a more advantageous method.

In addition, as BMI degradation by FeBDC-NH_2-activated PDS happened in aqueous solutions, the solution pH is a crucial factor. Fig. 6 (b) depicts the degradation of BMI by FeBDC-NH_2-activated PDS at various pH settings. At pH = 5, when the solution became slightly acidic, the rate of BMI degradation remained comparable to that at pH = 7, although the rate constant, *k*, fell to 0.039 min^{-1} (Fig. 6(d)). At pH = 3, when the solution became even more acidic, *k* reduced significantly to 0.07 min^{-1}, indicating that acid circumstances impeded BMI degradation by FeBDC-NH_2-activated PDS. This was possibly because PDS is more stable under acidic circumstances [41]; hence, PDS was difficult to activate, thereby inhibiting BMI degradation. In addition, FeBDC-NH_2 would be more positive on its surface (Fig. S4); thus, the electrostatic repulsion betwixt FeBDC-NH_2 and BMI grew stronger, hence preventing PDS activation by FeBDC-NH_2.

Besides, Fig. 6(b) demonstrates that BMI degradation was significantly altered in a moderately basic phase at pH = 9 and that the elimination rate was slightly more rapid at 0.059 min^{-1}. Possibly because the surface charge of FeBDC-NH2 was slightly negative (Fig. S4), the electrostatic attraction between the cationic BMI and FeBDC-NH2 grew greater, facilitating the interaction of BMI with the surface of FeBDC-NH2 where radicals were formed. However, after the pH reached 11, a highly alkaline state, BMI degradation appeared to be inhibited with a corresponding *k* = 0.011 min^{-1}. This was likely because PDS is prone to decomposing in basic phases with no generation of $SO4^{\bullet-}$ [42]. Consequently, little $SO4^{\bullet-}$ or other ROS would be available for BMI degradation. In addition, the concentration of OH^- in an alkaline environment negatively charged the surface of FeBDC-NH2, resulting in a significantly stronger electrostatic repulsion between $S2O8^{2-}$ and FeBDC-NH2. According to these findings, the optimal operational setting for BMI deterioration was a neutral or slightly alkaline environment.

3.5. Effects of salts on BMI degradation

As wastewaters frequently contain other components, these components would probably impact BMI elimination by PDS. Therefore, the influences of a ubiquitous salt, NaCl, and three common salts (e.g., $NaNO_3$, Na_2SO_4, and Na_3PO_4) on the elimination of BMI would be explored. Fig. 6(c) depicts BMI degradation by FeBDC-NH_2-activated PDS in the presence of NaCl; BMI degradation appeared to be marginally impacted, as the degradation kinetics slowed to 0.042 min^{-1} (Fig. 6(e)). Because NaCl would be dissociated into sodium and chloride ions, the chloride ion can react with $SO_4^{\bullet-}$ to form $Cl^{\bullet}$ and $Cl_2^{\bullet-}$, that have significantly smaller oxidation powers than $SO_4^{\bullet-}$ [43]. Moreover, when NO_3^{2-} was subsequently injected, the BMI elimination was also insignificantly influenced, as the *k* value reduced from 0.049 to 0.039 min^{-1}. Similar results are seen when SO_4^{2-} is present, with the BMI degrading at a rate of *k* = 0.035 min^{-1}. These ions may have deposited on the surface of FeBDC-NH_2 and interfered with the interactions between PDS and FeBDC-NH_2.

However, despite the fact that the presence of external ions may

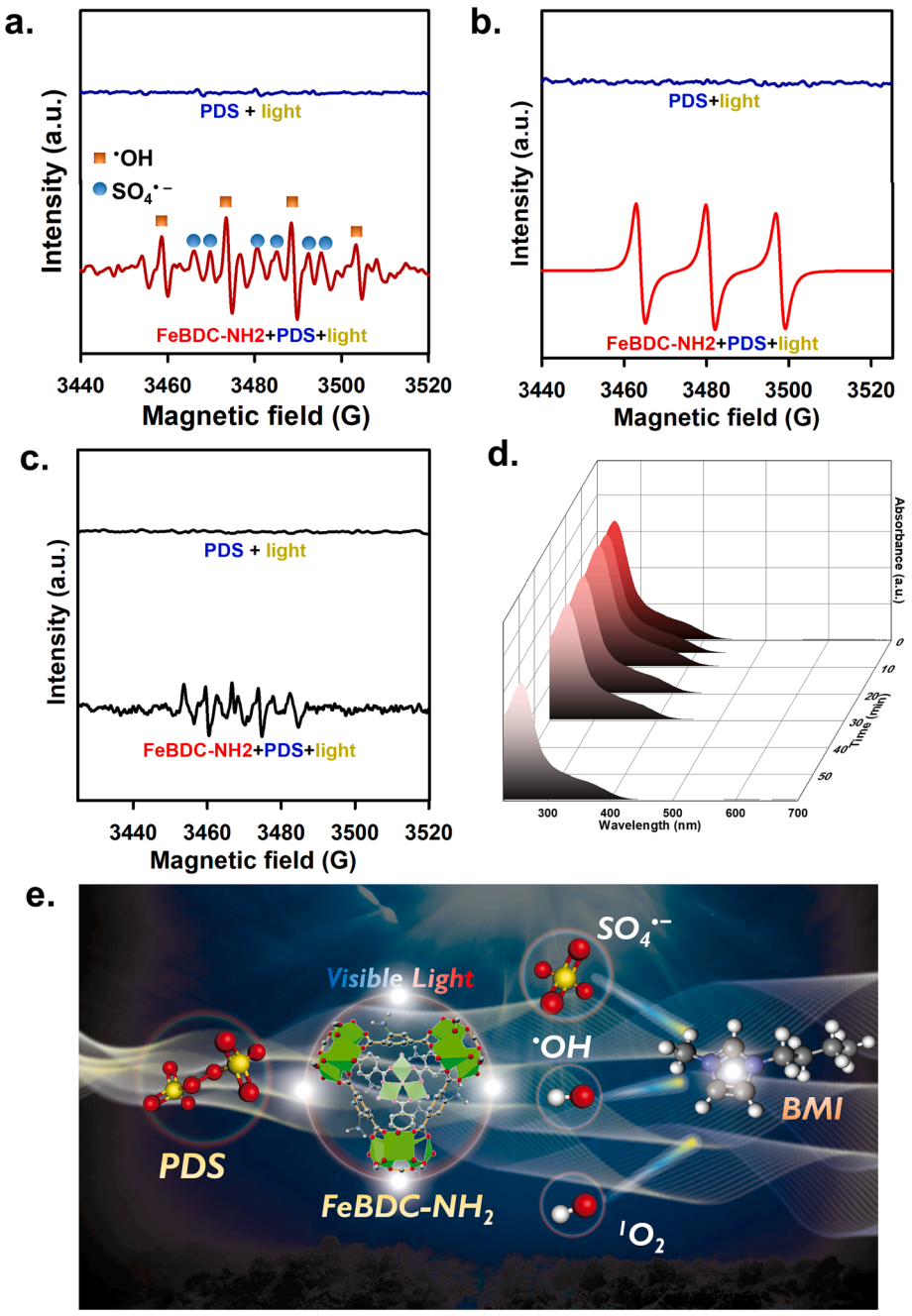

Fig. 8. ESR analyses: (a) DMPO, (b) TMP, (c) DMPO in methanol; (d) determination of superoxide by the NBT test.; (e) BMI degradation mechanism.

inhibit BMI degradation by FeBDC-NH_2, BMI was still degraded successfully after 60 min, suggesting that FeBDC-NH_2-activated PDS with light irradiation was a robust and effective approach for BMI elimination.

3.6. The reusability of FeBDC-NH_2 for activating PDS

It would be crucial for examining whether FeBDC-NH_2 was reusable for activating PDS for consecutive BMI elimination when exposed to light since FeBDC-NH_2 was proposed as a heterogeneous catalyst. According to Fig. 6(f), PDS activated by spent FeBDC-NH_2 could totally eliminate BMI after 60 min throughout several cycles, demonstrating that FeBDC-NH_2, even without regeneration, would still be robust and useful for activating PDS to destroy BMI when exposed to light.

To further examine if Fe would be released from FeBDC-NH_2 after the reusability test, the iron concentration from the multiple BMI elimination tests was determined as 0.003 mg/L using Inductively coupled plasma mass spectrometry. This confirmed that FeBDC-NH_2 would be robust as the amount of Fe released from FeBDC-NH_2 would be significantly smaller than the dose of FeBDC-NH_2 (e.g., 100 mg/L).

3.7. Degradation mechanism by FeBDC-NH_2 + PDS

A series of probe agents would then be examined to gain more knowledge of the ROS involved in BMI degradation. *Tert*-butanol (TBA) is used as a probe for $^{\bullet}OH$, whereas methanol can be used to detect $SO_4^{\bullet-}$ and $^{\bullet}OH$. When TBA was added, BMI degradation proceeded more slowly, and the rate constant decreased from 0.049 to 0.021 min^{-1} (Fig. 7(a-b))), indicating that $^{\bullet}OH$ may exist and contribute to BMI degradation. When methanol was used, the BMI degradation appeared

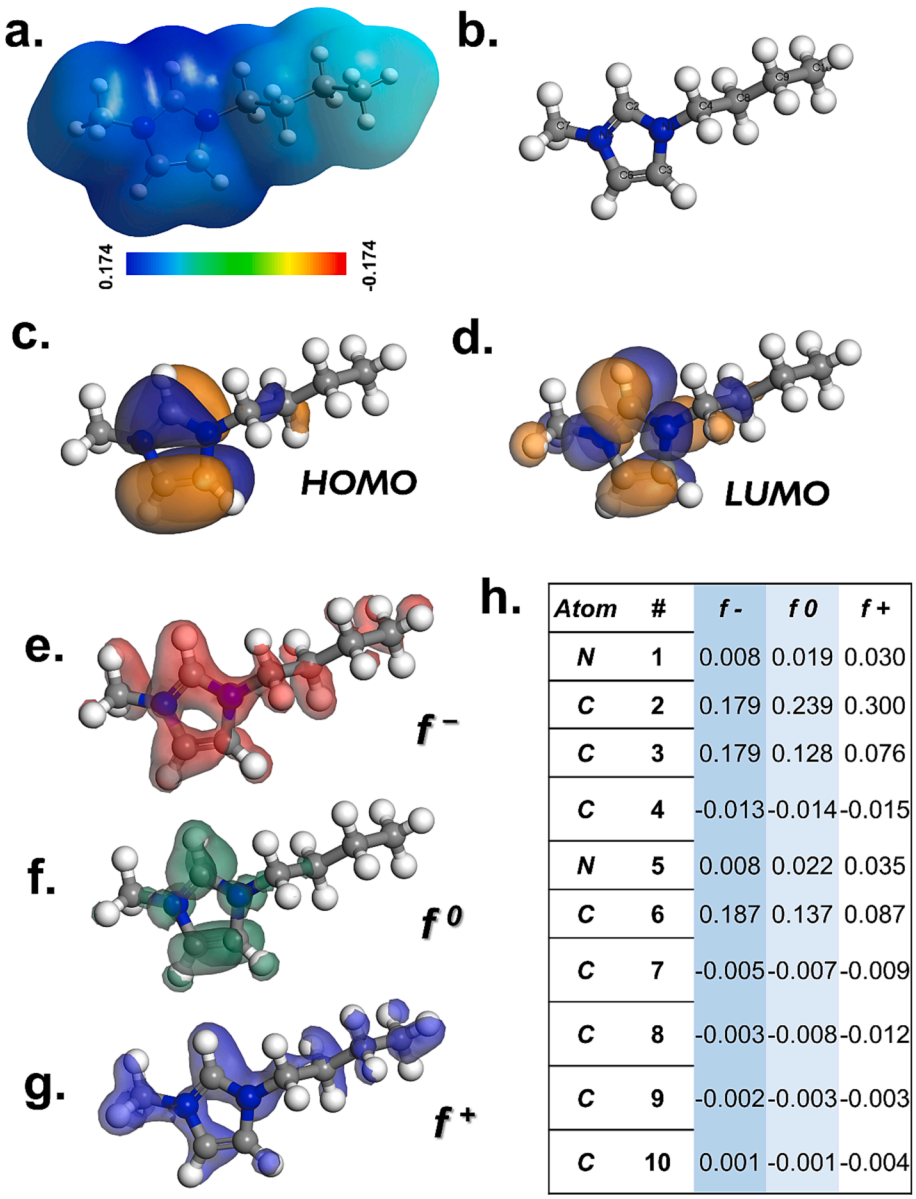

h.

Atom	#	f -	f 0	f +
N	1	0.008	0.019	0.030
C	2	0.179	0.239	0.300
C	3	0.179	0.128	0.076
C	4	-0.013	-0.014	-0.015
N	5	0.008	0.022	0.035
C	6	0.187	0.137	0.087
C	7	-0.005	-0.007	-0.009
C	8	-0.003	-0.008	-0.012
C	9	-0.002	-0.003	-0.003
C	10	0.001	-0.001	-0.004

Fig. 9. DFT calculation for BMI: (a) electrostatic potential (ESP), (b) the optimized molecule structure; (c) HOMO; (d) LUMO; and (e) condensed Fukui index distribution for electrophilic attack (f^-), (f) radical attack (f^0), and (g) nucleophilic attack (f^+); Fukui indices.

severely inhibited, as its k was only 0.006 min^{-1}, indicating that both $SO_4^{\bullet-}$ and $^{\bullet}OH$ may co-exist during BMI degradation. In addition, a second probe agent, benzoquinone (BQ), was utilized to determine the presence of superoxide ($O_2^{\bullet}$). Fig. 7(a) demonstrates that the presence of BQ caused BMI degradation to proceed much more slowly, with a k = 0.034 min^{-1}, possibly indicating that $O_2^{\bullet}$ may also be produced during BMI degradation. In addition, another probe agent, NaN_3, was used to investigate the presence of the non-radical species, singlet oxygen ($^1O_2$), and the introduction of NaN_3 also slowed BMI degradation with a k = 0.013 min^{-1}, indicating that $^1O_2$ also possibly occurred from FeBDC-NH_2-activated PDS under light irradiation during BMI degradation, and was involved in the non-radical pathway of degradation.

To determine reactive oxygen species (ROS), the existences of $SO_4^{\bullet-}$ and $^{\bullet}OH$ were analyzed using 2-HTPA and *p*-BQ, separately [44]. Analytic details are summarized in the supplementary materials. Fig. 5(a) demonstrates that the presence of 2-HTPA and p-BQ confirmed the presence of $SO_4^{\bullet-}$ and $^{\bullet}OH$, and the amounts of $SO_4^{\bullet-}$ and $^{\bullet}OH$ rose as the reaction time progressed. Nonetheless, the fraction of $SO_4^{\bullet-}$ appeared to be significantly higher than that of $^{\bullet}OH$, and this phenomenon was consistent with the previous assertion that $SO_4^{\bullet-}$ may be the principal species responsible for BMI degradation.

Furfuryl alcohol (FFA), which would react with $^1O_2$, could be used as a probe to detect the presence of $^1O_2$ instead. The presence of $^1O_2$ has been linked to the consumption of FFA. As shown in Fig. 7(d), PDS alone under light irradiation did not result in as much FFA consumption as did FeBDC-NH_2-activated PDS under light irradiation; therefore, the role of FeBDC-NH_2 in activating PDS to generate $^1O_2$ was positively determined. In general, PDS could be hydrolyzed to produce $^1O_2$, but the produced $^1O_2$ was insufficient and ineffective for degrading BMI. In contrast, the presence of FeBDC-NH would effectively activate PDS to generate $^1O_2$ for efficient BMI degradation.

Electron spin resonance (ESR) analysis would be acquired using 5,5-Dimethyl-1-pyrroline N-oxide (DMPO) and 2,2,6,6-tetramethylpiperidine (TMP) as spin-trapping agents to determine the actual species of ROS from FeBDC-NH_2 activated PDS under light irradiation during BMI degradation. Fig. 8(a) demonstrates that no discernible pattern was observed when DMPO was added in the absence of FeBDC-NH_2. Nonetheless, FeBDC-NH_2, and PDS under light irradiation with DMPO, a

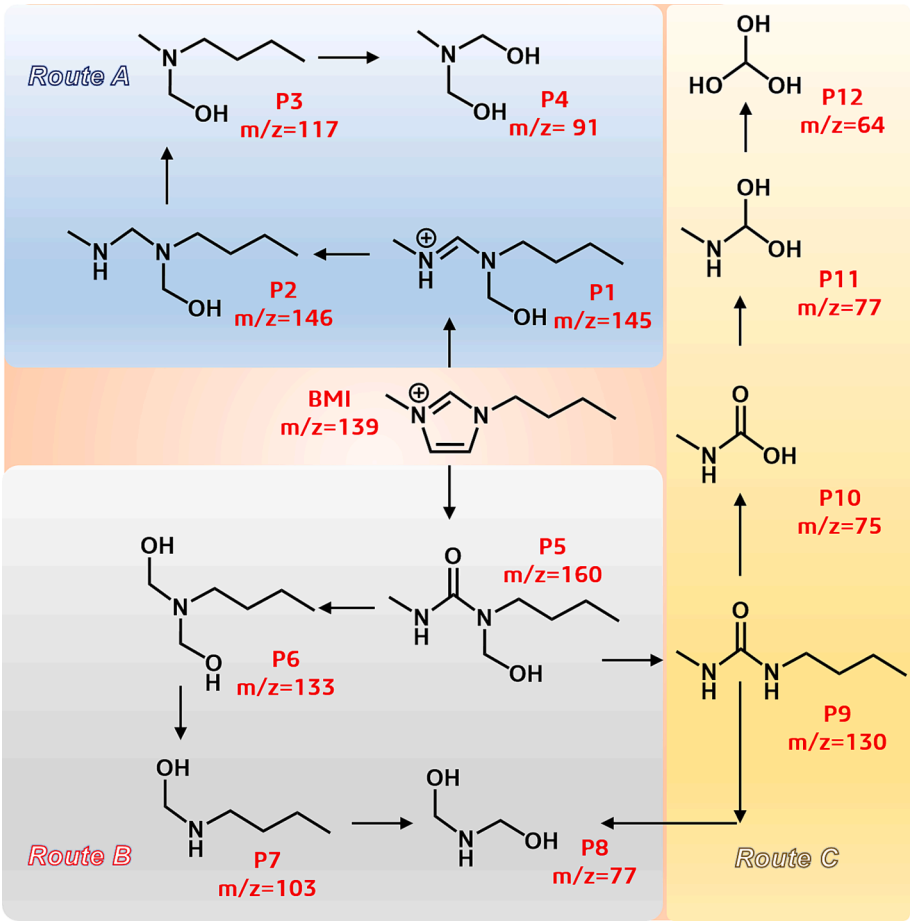

Fig. 10. A proposed degradation process of BMI by FeBDC-NH_2 + PDS + light based on the detected intermediates.

distinct pattern was observed and attributed to DMPO-SO_4 and DMPO-OH, as shown in Fig. 7(a). This demonstrates that $SO_4^{\bullet-}$ and $^{\bullet}OH$ were both present in the system of FeBDC-NH_2-activated PDS under light irradiation, contributing to the degradation of BMI.

In contrast, when TMP was adopted, insignificant detectable signals would be observed in the case of TMP and PDS. Once TMP, PDS, and FeBDC-NH_2 were introduced simultaneously; however, a special triplet pattern was observed and attributed to TMP-$^1O_2$, proving that $^1O_2$ existed and contributed to BMI degradation via the non-radical pathway.

The same experiment was repeated in methanol to determine if superoxide, $O_2^{\bullet-}$, would be generated from FeBDC-NH_2 activated PDS upon exposure to light. When DMPO and PDS were dissolved in methanol, essentially no signal was seen; however, when DMPO, PDS, and FeBDC-NH_2 were irradiated with light, a significant signal was obtained (Fig. 8 (b)). Nonetheless, the signal was interpreted as DMPO-X due to the oxidation of DMPO instead of $O_2^{\bullet-}$, suggesting that $O_2^{\bullet-}$ was not present in significant amounts during BMI degradation.

In addition, $O_2^{\bullet-}$ has been mentioned and may originate from PDS to partake in degradation [45]. To determine the presence of $O_2^{\bullet-}$, nitro blue tetrazolium (NBT) would be then selected as a probe because it possesses an ultraviolet absorption band at 260 nm, which could transform to a conventional formazan at 529 nm upon oxidation by $O_2^{\bullet-}$ [46]. Fig. 8(d) depicts a set of spectra at various reaction times; over 1 h, no noticeable band of formazan at 529 nm, indicating that $O_2^{\bullet-}$ was negligible. The relatively ineffective BMI elimination by the addition of BQ in the preceding section may be attributable to the fact that BQ can utilize more MPS without generating useful ROS [47] and also impede the approach of PDS to the surface of FeBDC-NH_2 [48].

These analyses additionally proved that BMI degradation by FeBDC-NH_2-activated PDS under light irradiation was unquestionably associated with multiple reactive oxygen species (ROS) (e.g., $SO_4^{\bullet-}$, $^{\bullet}OH$, $^1O_2$) as depicted in Fig. 8(e).

3.8. Degradation pathway of BMI by FeBDC-NH_2 activated PDS

Since BMI was successfully eliminated by FeBDC-NH_2-activated PDS, it would be worthwhile to investigate the degradation pathway of BMI. Here, the molecular orbitals (MOs) and Fukui indices were obtained from the density functional theory (DFT) calculation to provide insights into the potential reactive sites of BMI. At first glance, the electrostatic potential (ESP) map of BMI (Fig. 9(a)) reveals that areas near the imidazole ring of BMI are prone to withdrawing the attack from ROS. Next, the DFT-optimized structure of BMI is shown in Fig. 9(b), featuring atomic and numerical labeling. Fig. 9(c) displays its most highly occupied MO (HOMO), while Fig. 9(d) displays its most highly unoccupied MO (LUMO). The electron-poor and electron-rich regions of BMI are depicted by blue and orange balloons, respectively. In particular, BMI is vulnerable to electrophilic ROS such as $^{\bullet}OH$ because its HOMO on the imidazolate moiety is prone to losing electrons.

The distributions of the f^-, f^0, and f^+ are shown in Fig. 9(f), (g), and (h), separately, along with the Fukui indices of BMI that were also calculated. A large Fukui index value often indicates that an atom is more likely to be the target of attacks. Because a site with a high f^- value might more likely attract electrophilic attacks, C6, which has the highest f^-, would be the most vulnerable target. Additionally, C2, C3, and other atoms showed larger f^- values; as a result, these sites are vulnerable to attacks at the start of BMI decomposition. One of the strongest electrophilic species is $^1O_2$, and both $SO_4^{\bullet-}$ and $^{\bullet}OH$ are thought to exhibit electrophilic characteristics. As a result, the HOMO found at these BMI

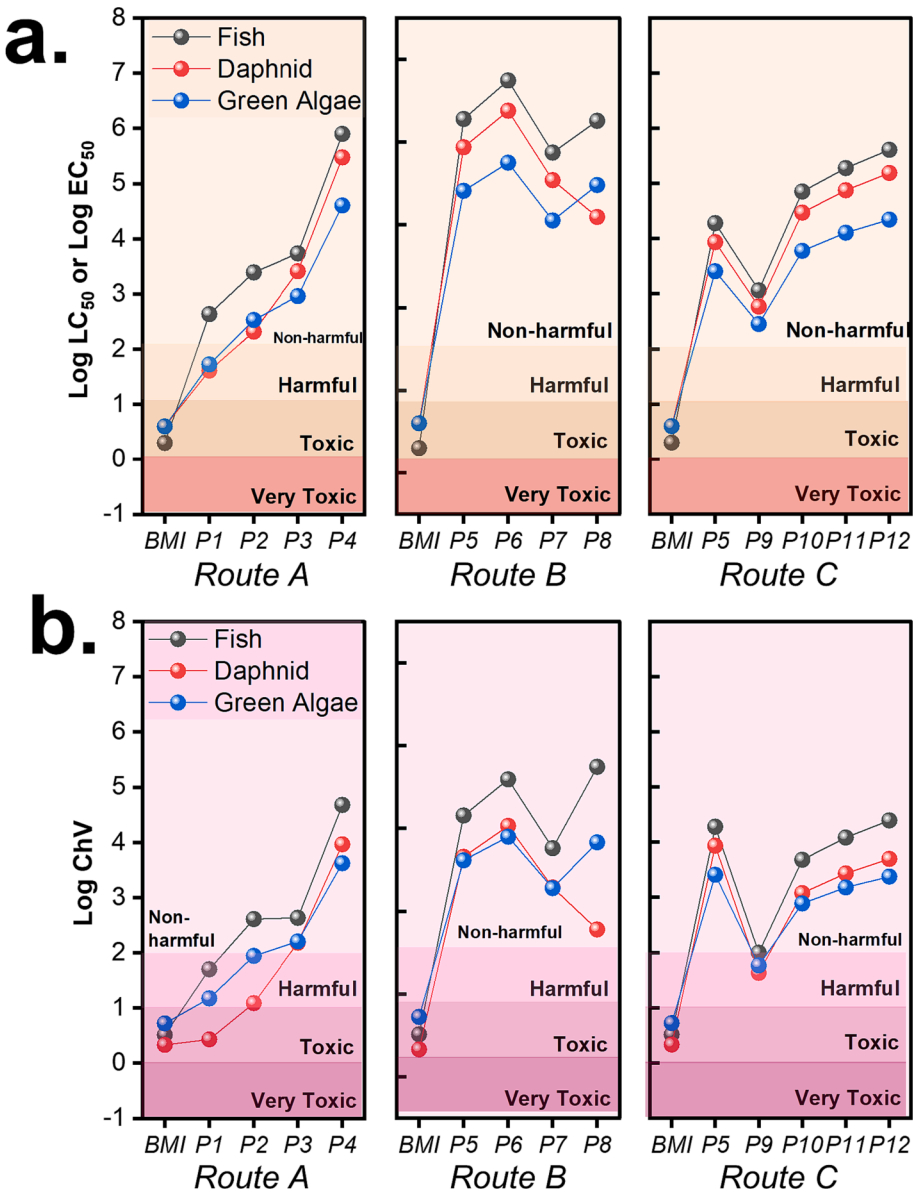

Fig. 11. Estimated aquatic toxicities of BMI and its degradation intermediates: (a) acute toxicity and (b) chronic toxicity.

locations appeared to be susceptible to electrophilic attacks from these ROS.

In addition, the f^0 indices that can be used to identify atoms that are likely to be attacked by radicals are shown in Fig. 9(e) and (g). Maximum probability of receiving radical attacks is highest for C2, followed by C6 and C3. These studies suggest that assaults on the imidazolate ring at C6, C2, and C3 could be the starting point for BMI decomposition.

Mass spectrometry analysis of the decomposition of BMI by FeBDC-NH2 activated PDS under light irradiation is shown in Fig. S5, and a summary of the identified intermediates is provided in Table S1. Given these molecules and results from computer investigations, Fig. 10 depicts a potential decomposition pathway for BMI by FeBDC-NH_2 activated PDS in the presence of light.

Initially, the imidazole ring of BMI might receive attacks at the positions of C6 or C3 to undergo a ring-opening reaction, affording an intermediate, P1, which would then evolve into P2. With additional attacks, the secondary amine group of P2 might be eliminated to produce P3, which would be further oxidized to degrade its alkyl chain to generate P4. On the other hand, after receiving the ring-opening reaction, BMI could be also decomposed to generate P5, which would be further degraded to eliminate the secondary amine group for producing P6. Next, P6 would be then oxidized to remove the ethanol group or decompose the alkyl chain to produce P7 and P8, respectively. Simultaneously, the intermediate P5 might be decomposed to eliminate its ethanol group to generate P9, which would be then oxidized to degrade its alkyl chain, affording P10. Through continuous attacks, P10 would be then decomposed to afford P11 and P12. Alternatively, P9 might be also oxidized and decomposed to afford P8. According to these intermediates, the overall BMI degradation process can be then illustrated via three routes: the route A, B, and C as indicated in Fig. 10.

3.9. Eco-toxicity evaluation of BMI degradation intermediates

In view of the degradation pathway of BMI by FeBDC-NH_2 activated PDS under light irradiation, it was also crucial to evaluate the eco-toxicity of intermediates generated from BMI degradation especially for aquatic life. Herein, The Ecological Structure Activity Relationships (ECOSAR) Class Program from the United States Environmental Protection Agency was adopted to evaluate acute and chronic toxicities of these intermediates towards fish, daphnid and green algae. Based on the

Globally Harmonized System of Classification and Labelling of Chemicals (Table S2), the data of LC_{50}/EC_{50}/ChV of these intermediates from the ECOSAR could be then categorized into the four levels of toxicity (i.e., very toxic, toxic, harmful and non-harmful). Fig. 11(a) displays values of Log LC_{50}/EC_{50} of these intermediates on the three degradation routes. In the case of the route A, the acute toxicity of BMI was actually notable as it was classified to be "Toxic". Once BMI was degraded to P1, the corresponding toxicity has been considerably reduced to be "non-harmful" and "harmful". After P1 was further decomposed to become P2, P3, and P4, the toxicities of these compounds have been tremendously decreased, making these intermediates "non-harmful". In the case of the route B, after BMI is oxidized to produce P5, its corresponding toxicity has been substantially decreased to be non-harmful. The derivatives of P5 into P6, P7, and P8 are also found to be "non-harmful" with insignificant acute toxicities. Moreover, in the case of the route C, after BMI is decomposed into P5, the derivatives of P5 into P9, P10, and P11, are also found to exhibit very low acute toxicities, making these intermediates as "non-harmful" compounds. These analyses demonstrate that the degradation of BMI by FeBDC-NH_2 activated-PDS under light irradiation would successfully and effectively reduce toxicities of BMI and the derivatives of BMI along the degradation process are non-harmful in terms of acute toxicities.

Fig. 11(b) displays values of Log ChV, the chronic toxicity, of these intermediates on the three degradation routes. In the case of the route A, the chronic toxicity of BMI is also significant as it can be classified to be "Toxic". Once BMI was degraded to P1, the corresponding chronic toxicity has been considerably reduced to be "harmful". After P1 was further decomposed to become P2, its chronic toxicity has been slightly decreased, making these intermediates "harmful" and "non-harmful". However, after P2 was further decomposed to become P3 and P4, the chronic toxicities of these compounds have been tremendously decreased, making these intermediates "non-harmful".

In the case of the route B, after BMI is oxidized to produce P5, its corresponding toxicity has been substantially decreased to be non-harmful. The derivatives of P5 into P6, P7, and P8 are also found to be "non-harmful" with insignificant chronic toxicities. Moreover, in the case of the route C, after BMI is decomposed into P5, the derivatives of P5 into P9 is found to exhibit slightly-increased toxicity but the derivatives of P9 into P10, P11 and P12 exhibit very low chronic toxicities, making these intermediates as "non-harmful" compounds. These analyses demonstrate that the degradation of BMI by FeBDC-NH_2 activated PDS under light irradiation would successfully and effectively reduce toxicities of BMI and the final derivatives of BMI along the degradation process are non-harmful in terms of both acute and chronic toxicities.

4. Conclusions

While both FeBDC and FeBDC-NH_2 can activate PDS to degrade BMI, FeBDC-NH_2 can lead to a considerable enhancement in BMI degradation under visible light irradiation. The activation energy of BMI degradation as 30.7 kJ/mol is also significantly lower than the reported values by other oxidation approaches. Here, we use theoretical DFT calculations to explore the activation mechanism and degradation pathway of BMI degradation by FeBDC-NH_2/PDS. The corresponding acute and chronic eco-toxicities of degradation intermediates of BMI are also studied to realize the degradation implication of BMI. These analyses demonstrate that the degradation of BMI by FeBDC-NH_2 activated PDS under light irradiation would successfully and effectively reduce toxicities of BMI and the final derivatives of BMI along the degradation process are non-harmful in terms of both acute and chronic toxicities.

CRediT authorship contribution statement

Tran Doan Trang: Data curation, Writing – original draft. **Eilhann Kwon:** Data curation. **Jet-Chau Wen:** Data curation. **Nguyen Nhat Huy:** Data curation, Visualization, Investigation. **Venkata Subbaiah Munagapati:** Data curation. **Suresh Ghotekar:** Data curation, Visualization, Investigation. **Kuo-Pin Yu:** Writing – original draft. **Kun-Yi Andrew Lin:** Writing – original draft.

Declaration of Competing Interest

The authors declare that they have no known competing financial interests or personal relationships that could have appeared to influence the work reported in this paper.

Data availability

The authors are unable or have chosen not to specify which data has been used.

Appendix A. Supplementary material

Supplementary data to this article can be found online at https://doi.org/10.1016/j.molliq.2023.122832.

References

[1] H. Olivier-Bourbigou, L. Magna, D. Morvan, Ionic liquids and catalysis: Recent progress from knowledge to applications, Appl. Catal. A 373 (2010) 1–56.
[2] A.P.M. Tavares, B. Pinho, O. Rodriguez, E.A. Macedo, Biocatalysis in Ionic Liquid: Degradation of Phenol by Laccase, Procedia Eng. 42 (2012) 226–230.
[3] A. Oskarsson, M.C. Wright, Ionic Liquids: New Emerging Pollutants, Similarities with Perfluorinated Alkyl Substances (PFASs), Environ. Sci. Tech. 53 (2019) 10539–10541.
[4] T.P. Thuy Pham, C.-W. Cho, Y.-S. Yun, Environmental fate and toxicity of ionic liquids: A review, Water Res. 44 (2010) 352–372.
[5] C.P. Fredlake, J.M. Crosthwaite, D.G. Hert, S.N.V.K. Aki, J.F. Brennecke, Thermophysical Properties of Imidazolium-Based Ionic Liquids, J. Chem. Eng. Data 49 (2004) 954–964.
[6] A. Kurata, S. Shimizu, Y. Shiraishi, M. Abe, N. Naito, M. Shimada, N. Kishimoto, Degradation of ionic liquids by a UV/H2O2 process and CMCase from novel ionic liquid-tolerant alkaliphilic Nocardiopsis sp. SSC4, Biotechnol. Biotechnol. Equip. 31 (2017) 749–755.
[7] E.M. Siedlecka, W. Mrozik, Z. Kaczyński, P. Stepnowski, Degradation of 1-butyl-3-methylimidazolium chloride ionic liquid in a Fenton-like system, J. Hazard. Mater. 154 (2008) 893–900.
[8] P.A. Hunt, B. Kirchner, T. Welton, Characterising the Electronic Structure of Ionic Liquids: An Examination of the 1-Butyl-3-Methylimidazolium Chloride Ion Pair 12 (2006) 6762–6775.
[9] S. Satyen, H. Satoshi, K. Akiko, H. Hiro-o, Crystal Structure of 1-Butyl-3-methylimidazolium Chloride, A Clue to the Elucidation of the Ionic Liquid Structure 32 (2003) 740–741.
[10] M. Munoz, C.M. Domínguez, Z.M. de Pedro, A. Quintanilla, J.A. Casas, J. J. Rodriguez, Ionic liquids breakdown by Fenton oxidation, Catal. Today 240 (2015) 16–21.
[11] E.M. Siedlecka, M. Go3ębiowski, J. Kumirska, P. Stepnowski, Identification of 1-Butyl-3-methylimidazolium Chloride Degradation Products Formed in Fe(III)/H2O2 Oxidation System, Chem. Anal. 53 (2008) 934–951.
[12] C.M. Domínguez, M. Munoz, A. Quintanilla, Z.M. de Pedro, S.P.M. Ventura, J.A. P. Coutinho, J.A. Casas, J.J. Rodriguez, Degradation of imidazolium-based ionic liquids in aqueous solution by Fenton oxidation, J. Chem. Technol. Biotechnol. 89 (2014) 1197–1202.
[13] M. Munoz, C.M. Domínguez, Z.M. de Pedro, A. Quintanilla, J.A. Casas, S.P. M. Ventura, J.A.P. Coutinho, Role of the chemical structure of ionic liquids in their ecotoxicity and reactivity towards Fenton oxidation, Sep. Purif. Technol. 150 (2015) 252–256.
[14] M.G. Antoniou, A.A. de la Cruz, D.D. Dionysiou, Degradation of microcystin-LR using sulfate radicals generated through photolysis, thermolysis and e− transfer mechanisms, Appl. Catal. B 96 (2010) 290–298.
[15] J. Lee, U. von Gunten, J.-H. Kim, Persulfate-Based Advanced Oxidation: Critical Assessment of Opportunities and Roadblocks, Environ. Sci. Tech. 54 (2020) 3064–3081.
[16] L.W. Matzek, K.E. Carter, Activated persulfate for organic chemical degradation: A review, Chemosphere 151 (2016) 178–188.
[17] T. Wang, C. Zhao, L. Meng, Y. Li, D. Wang, C.-C. Wang, Fe−O−P bond in MIL-88A (Fe)/BOHP heterojunctions as a highway for rapid electron transfer to enhance photo-Fenton abatement of enrofloxacin, Appl. Catal. B 334 (2023), 122832.
[18] Y.-H. Li, C.-C. Wang, F. Wang, W. Liu, L. Chen, C. Zhao, H. Fu, P. Wang, X. Duan, Nearly zero peroxydisulfate consumption for persistent aqueous organic pollutants degradation via nonradical processes supported by in-situ sulfate radical regeneration in defective MIL-88B(Fe), Appl. Catal. B 331 (2023), 122699.
[19] C. Zhao, L. Meng, H. Chu, J.-F. Wang, T. Wang, Y. Ma, C.-C. Wang, Ultrafast degradation of emerging organic pollutants via activation of peroxymonosulfate

over Fe3C/Fe@N-C-x: Singlet oxygen evolution and electron-transfer mechanisms, Appl. Catal. B 321 (2023), 122034.
[20] D. Ding, C. Liu, Y. Ji, Q. Yang, L. Chen, C. Jiang, T. Cai, Mechanism insight of degradation of norfloxacin by magnetite nanoparticles activated persulfate: Identification of radicals and degradation pathway, Chem. Eng. J. 308 (2017) 330–339.
[21] X. Chen, J. Chen, X. Qiao, D. Wang, X. Cai, Performance of nano-Co3O4/peroxymonosulfate system: Kinetics and mechanism study using Acid Orange 7 as a model compound, Appl Catal B 80 (2008) 116–121.
[22] K.-Y. Andrew Lin, S.-Y. Chen, Bromate reduction in water by catalytic hydrogenation using metal-organic frameworks and sodium borohydride, RSC Adv. 5 (2015) 43885–43896.
[23] N.A. Ramsahye, T.K. Trung, L. Scott, F. Nouar, T. Devic, P. Horcajada, E. Magnier, O. David, C. Serre, P. Trens, Impact of the Flexible Character of MIL-88 Iron(III) Dicarboxylates on the Adsorption of n-Alkanes, Chem. Mater. 25 (2013) 479–488.
[24] Z. Zhang, X. Li, B. Liu, Q. Zhao, G. Chen, Hexagonal microspindle of NH2-MIL-101 (Fe) metal-organic frameworks with visible-light-induced photocatalytic activity for the degradation of toluene, RSC Adv. 6 (2016) 4289–4295.
[25] Q. Xie, Y. Li, Z. Lv, H. Zhou, X. Yang, J. Chen, H. Guo, Effective Adsorption and Removal of Phosphate from Aqueous Solutions and Eutrophic Water by Fe-based MOFs of MIL-101, Sci. Rep. 7 (2017) 3316.
[26] K.-Y.-A. Lin, J.-T. Lin, A.P. Jochems, Oxidation of amaranth dye by persulfate and peroxymonosulfate activated by ferrocene, J. Chem. Technol. Biotechnol. 92 (2017) 163–172.
[27] J. Liu, T. Zhang, Z. Wang, G. Dawson, W. Chen, Simple pyrolysis of urea into graphitic carbon nitride with recyclable adsorption and photocatalytic activity, J. Mater. Chem. 21 (2011) 14398–14401.
[28] Y. Bao, K. Chen, AgCl/Ag/g-C3N4 Hybrid Composites: Preparation Visible Light-Driven Photocatalytic Activity and Mechanism, Nano-Micro Letters 8 (2016) 182–192.
[29] J. Yan, C. Zhou, P. Li, B. Chen, S. Zhang, X. Dong, F. Xi, J. Liu, Nitrogen-rich graphitic carbon nitride: Controllable nanosheet-like morphology, enhanced visible light absorption and superior photocatalytic performance, Colloids Surf. Physicochem. Eng. Aspects 508 (2016) 257–264.
[30] D. Wang, R. Huang, W. Liu, D. Sun, Z. Li, Fe-Based MOFs for Photocatalytic CO2 Reduction: Role of Coordination Unsaturated Sites and Dual Excitation Pathways, ACS Catal. 4 (2014) 4254–4260.
[31] S. Rodriguez, L. Vasquez, D. Costa, A. Romero, A. Santos, Oxidation of Orange G by persulfate activated by Fe(II), Fe(III) and zero valent iron (ZVI), Chemosphere 101 (2014) 86–92.
[32] A. Behnami, E. Aghayani, K.Z. Benis, M. Sattari, M. Pourakbar, Comparing the efficacy of various methods for sulfate radical generation for antibiotics degradation in synthetic wastewater: degradation mechanism, kinetics study, and toxicity assessment, RSC Adv. 12 (2022) 14945–14956.
[33] X.-Y. Jiang, E. Kwon, H.-C. Chang, N.N. Huy, X. Duan, S. Ghotekar, Y.-C. Tsai, A. Ebrahimi, F. Ghanbari, K.-Y. Andrew Lin, Tuning nanostructured CuCo2O4 on 3D macro-support for enhanced degradation of carbofuran via catalytic activation monopersulfate: Key roles of morphology and active species, Sep. Purif. Technol., 308 (2023) 122789.
[34] T.C. Khiem, N.N. Huy, E. Kwon, X. Duan, S. Wacławek, J. Bedia, Y.-C. Tsai, A. Ebrahimi, F. Ghanbari, K.-Y.-A. Lin, Hetero-interface-engineered sulfur vacancy and oxygen doping in hollow Co9S8/Fe7S8 nanospheres towards monopersulfate activation for boosting intrinsic electron transfer in paracetamol degradation, Appl. Catal. B 330 (2023), 122550.
[35] T.C. Khiem, N.N. Huy, T.D. Trang, J.-C. Wen, E. Kwon, H.-C. Chang, C. Hu, X. Duan, K.-Y.-A. Lin, Boosting elimination of sunscreen, Tetrahydroxybenzophenone (BP-2), from water using monopersulfate activated by thorny NanoBox of Co@C prepared via the engineered etching strategy: A comparative and mechanistic investigation, Chemosphere 327 (2023), 138469.
[36] W.-J. Liu, Y.-K. Park, H.M. Bui, N.N. Huy, C.-H. Lin, S. Ghotekar, T. Wi-Afedzi, K.-Y.-A. Lin, Hofmann-MOF-derived CoFeNi nanoalloy@CNT as a magnetic activator for peroxymonosulfate to degrade benzophenone-1 in water, J. Alloy. Compd. 937 (2023), 165189.
[37] Y. Fu, D. Sun, Y. Chen, R. Huang, Z. Ding, X. Fu, Z. Li, An Amine-Functionalized Titanium Metal-Organic Framework Photocatalyst with Visible-Light-Induced Activity for CO2 Reduction, Angew. Chem. Int. Ed. 51 (2012) 3364–3367.
[38] C.-B. Chen, F. Zhang, C.-X. Li, J.-Y. Lu, S. Cui, H.-Q. Liu, W.-W. Li, A magnetic CoFe2O4-CNS nanocomposite as an efficient, recyclable catalyst for peroxymonosulfate activation and pollutant degradation, RSC Adv. 7 (2017) 55020–55025.
[39] Y. Pi, L. Ma, P. Zhao, Y. Cao, H. Gao, C. Wang, Q. Li, S. Dong, J. Sun, Facile green synthetic graphene-based Co-Fe Prussian blue analogues as an activator of peroxymonosulfate for the degradation of levofloxacin hydrochloride, J. Colloid Interface Sci. 526 (2018) 18–27.
[40] C.M. Domínguez, M. Munoz, A. Quintanilla, Z.M. de Pedro, J.A. Casas, Kinetics of imidazolium-based ionic liquids degradation in aqueous solution by Fenton oxidation, Environ. Sci. Pollut. Res. 25 (2018) 34811–34817.
[41] W. Guo, S. Su, C. Yi, Z. Ma, Degradation of antibiotics amoxicillin by Co3O4-catalyzed peroxymonosulfate system, Environ. Prog. Sustain. Energy 32 (2013) 193–197.
[42] A. Rastogi, S.R. Al-Abed, D.D. Dionysiou, Sulfate radical-based ferrous–peroxymonosulfate oxidative system for PCBs degradation in aqueous and sediment systems, Appl. Catal. B 85 (2009) 171–179.
[43] F. Qi, W. Chu, B. Xu, Modeling the heterogeneous peroxymonosulfate/Co-MCM41 process for the degradation of caffeine and the study of influence of cobalt sources, Chem. Eng. J. 235 (2014) 10–18.
[44] W.D. Oh, Z. Dong, G. Ronn, T.T. Lim, Surface-active bismuth ferrite as superior peroxymonosulfate activator for aqueous sulfamethoxazole removal: Performance, mechanism and quantification of sulfate radical, J. Hazard. Mater. 325 (2017) 71–81.
[45] H.-H. Chen, Y.-K. Park, E. Kwon, Y. Fai Tsang, B. Xuan Thanh, T. Cong Khiem, S. You, C. Hu, K.-Y.-A. Lin, Nanoneedle-Assembled Copper/Cobalt sulfides on nickel foam as an enhanced 3D hierarchical catalyst to activate monopersulfate for Rhodamine b degradation, J. Colloid Interface Sci. 613 (2022) 168–181.
[46] X. Ma, H. Cheng, Facet-dependent photocatalytic H2O2 production of single phase Ag3PO4 and Z-scheme Ag/ZnFe2O4-Ag-Ag3PO4 composites, Chem. Eng. J. 429 (2022), 132373.
[47] Y. Zhou, J. Jiang, Y. Gao, J. Ma, S.-Y. Pang, J. Li, X.-T. Lu, L.-P. Yuan, Activation of Peroxymonosulfate by Benzoquinone: A Novel Nonradical Oxidation Process, Environ. Sci. Tech. 49 (2015) 12941–12950.
[48] T.C. Khiem, D.D. Tuan, E. Kwon, N.N. Huy, W.-D. Oh, W.-H. Chen, K.-Y.-A. Lin, Degradation of dihydroxybenzophenone through monopersulfate activation over nanostructured cobalt ferrites with various morphologies: A comparative study, Chem. Eng. J. 450 (2022), 137798.